Electronic Supplementary Material (ESI) for Physical Chemistry Chemical Physics.

Supplementary information

Effect of transition metal cations on the local structure and lithium transport in disordered rock-salt oxides

D.O. Semykina[a], Ye.A. Morkhova [a,b,c], A.A. Kabanov[a,b,d], K.V. Mishchenko[a], A.B. Slobodyuk[a,e], M.A. Kirsanova[f], O.A. Podgornova[a], A.A. Shindrov[a], K.S. Okhotnikov[g], N.V. Kosova[a*]

[a]*Institute of Solid State Chemistry and Mechanochemistry SB RAS, 18 Kutateladze, 630128 Novosibirsk, Russia*
[b]*Samara State Technical University, Molodogvardeyskaya St. 244, 443100 Samara, Russia*
[c]*Samara University, Academician Pavlov Str. 1, 443011 Samara, Russia*
[d]*P.N. Lebedev Physical Institute of the Russian Academy of Sciences, Novo-Sadovaya Str. 18, 443011 Samara, Russia*
[e]*Institute of Chemistry, Far-Eastern Branch of the Russian Academy of Sciences, 159 pr. Stoletiya Vladivostoka, 690022 Vladisvostok, Russia*
[f]*Skolkovo Institute of Science and Technology, 3 Nobel str., 121205 Moscow, Russia*
[g]*Independent researcher*

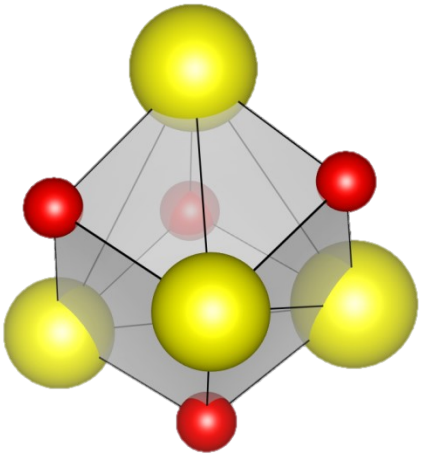

Fig. S1. A tetrahedral environment of a void can be determined using either oxygen atoms (red spheres) or metal atoms (yellow spheres) at the vertices. The second description is utilized in the present paper. When all the metals are Li^+ such an environment is referred to as 0TM.

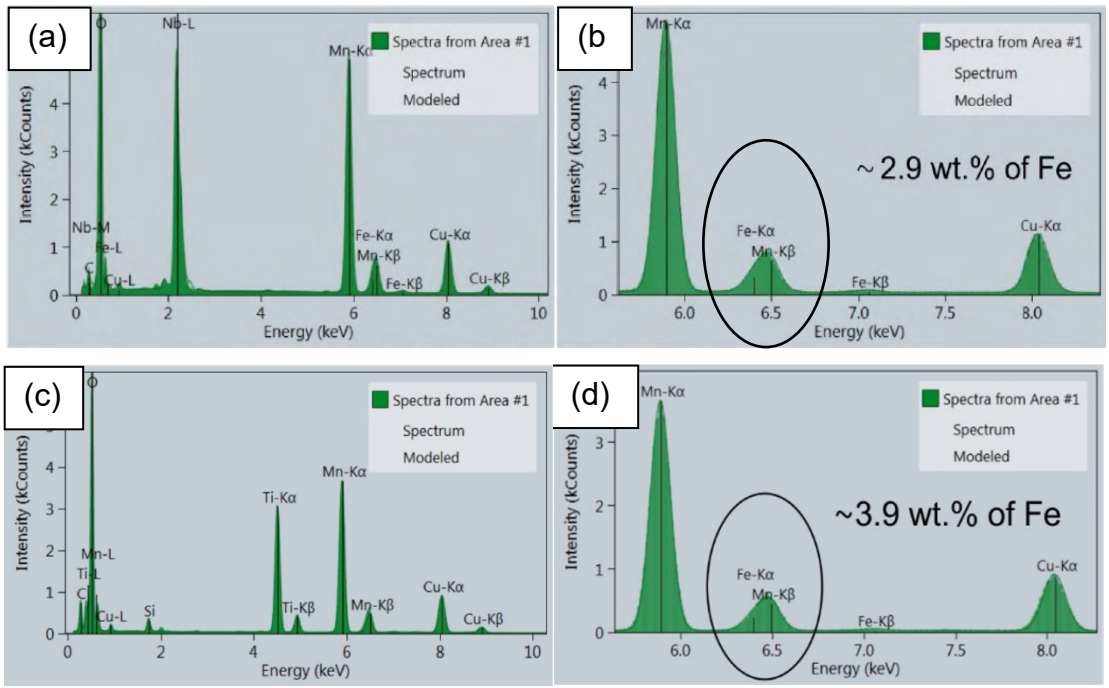

Fig. S2. Energy dispersive X-ray spectra of the $Li_{1.3}Nb_{0.3}Mn_{0.4}O_2$ (a, b) and $Li_{1.2}Ti_{0.4}Mn_{0.4}O_2$ (c, d) samples after annealing. Careful analysis of Mn-Kβ line in the spectra reveals the weak low-energy shoulder, which can be assigned to Fe-Kα with energy of 6.4 keV. Deconvolution of EDX spectrum with Fe lines gives perfect fit between experimental and modeled spectra and Fe content of ca. 3-4 wt. %.

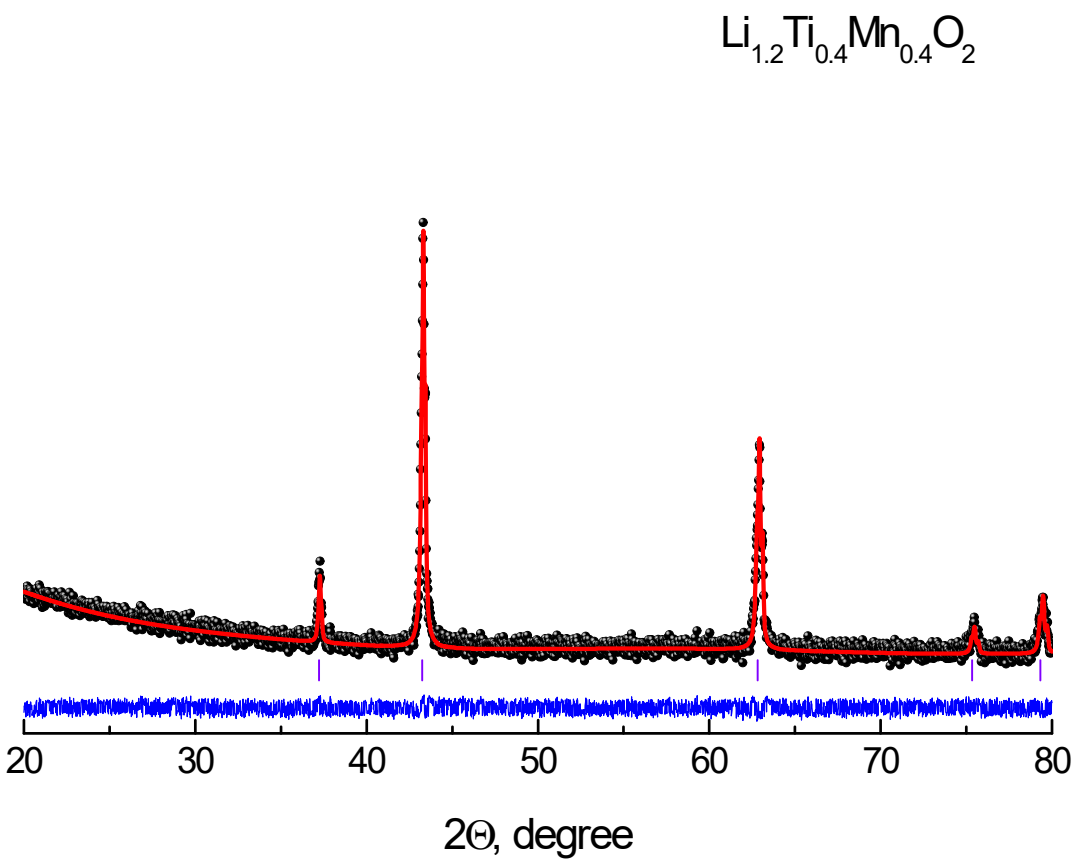

Fig. S3. Rietveld refinement of the structure of $Li_{1.2}Ti_{0.4}Mn_{0.4}O_2$.

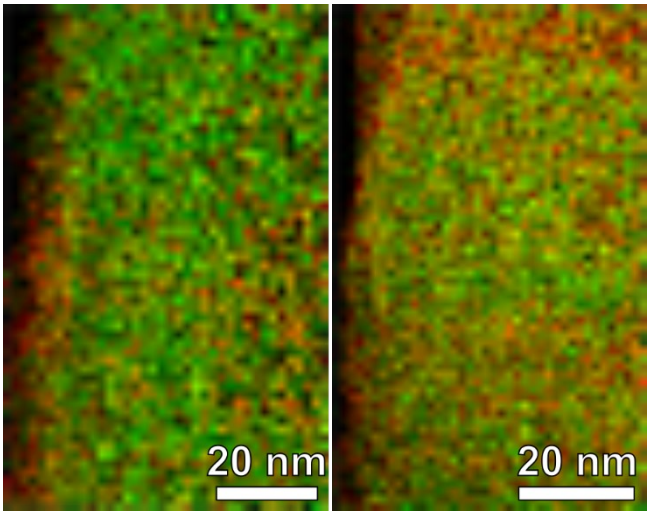

Fig. S4. STEM-EELS maps of $Mn^{2+,3+}$ (red) and $Mn^{3+,4+}$ (green) states recorded from crystals of $Li_{1.3}Nb_{0.3}Mn_{0.4}O_2$.

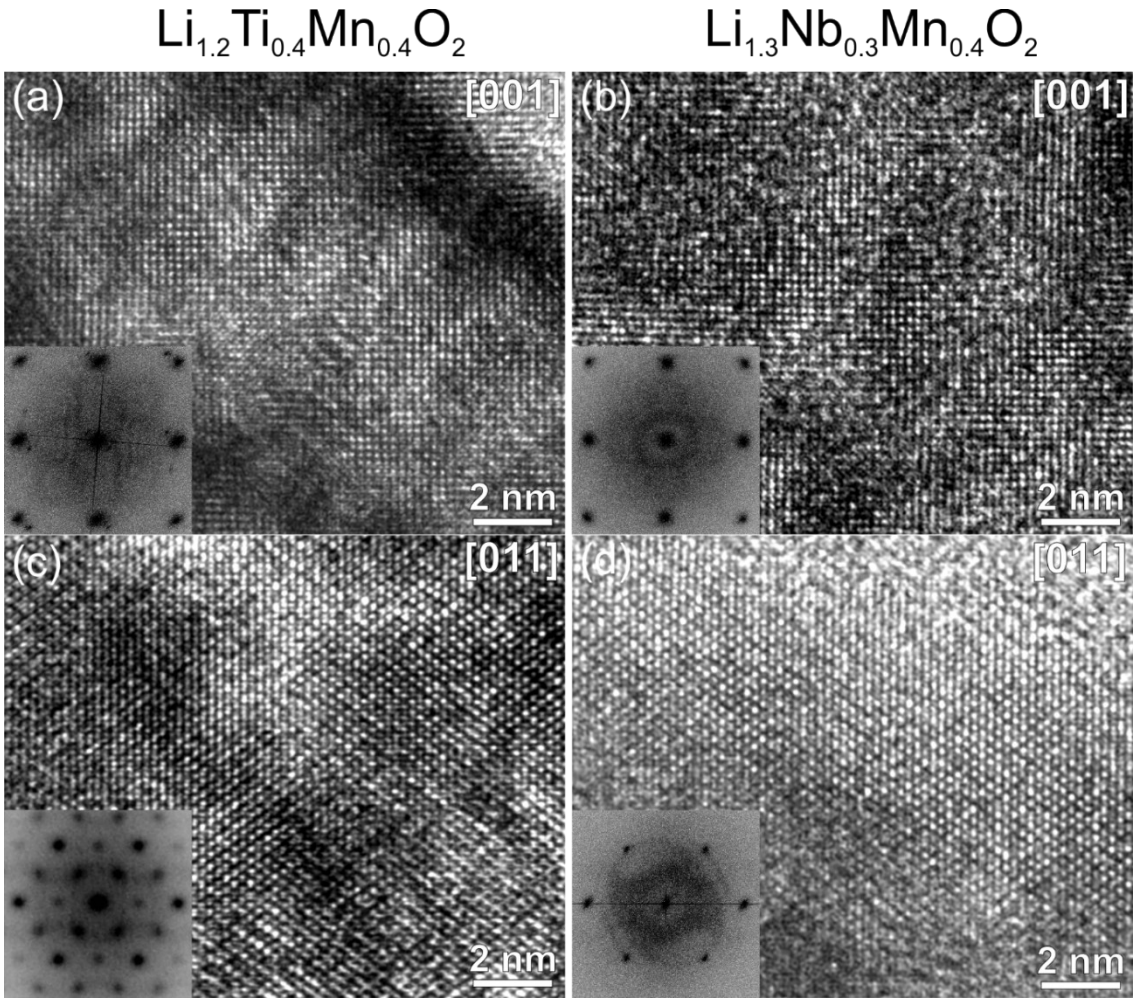

Fig. S5. High-resolution [001] and [011] BF-TEM images of $Li_{1.2}Ti_{0.4}Mn_{0.4}O_2$ (a, c) $Li_{1.3}Nb_{0.3}Mn_{0.4}O_2$ (b, d). The Fourier-transforms are shown as insets.

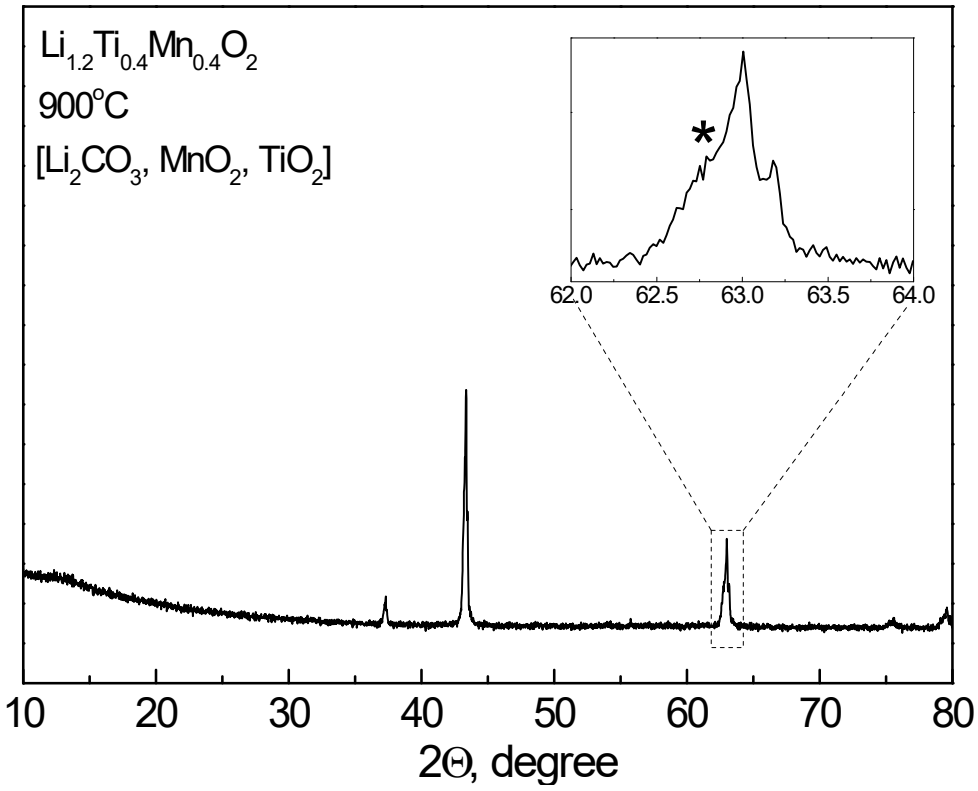

Fig. S6. The example of superstructure observed by XRD on the sample prepared from lithium carbonate instead of oxide and at lower annealing temperature.

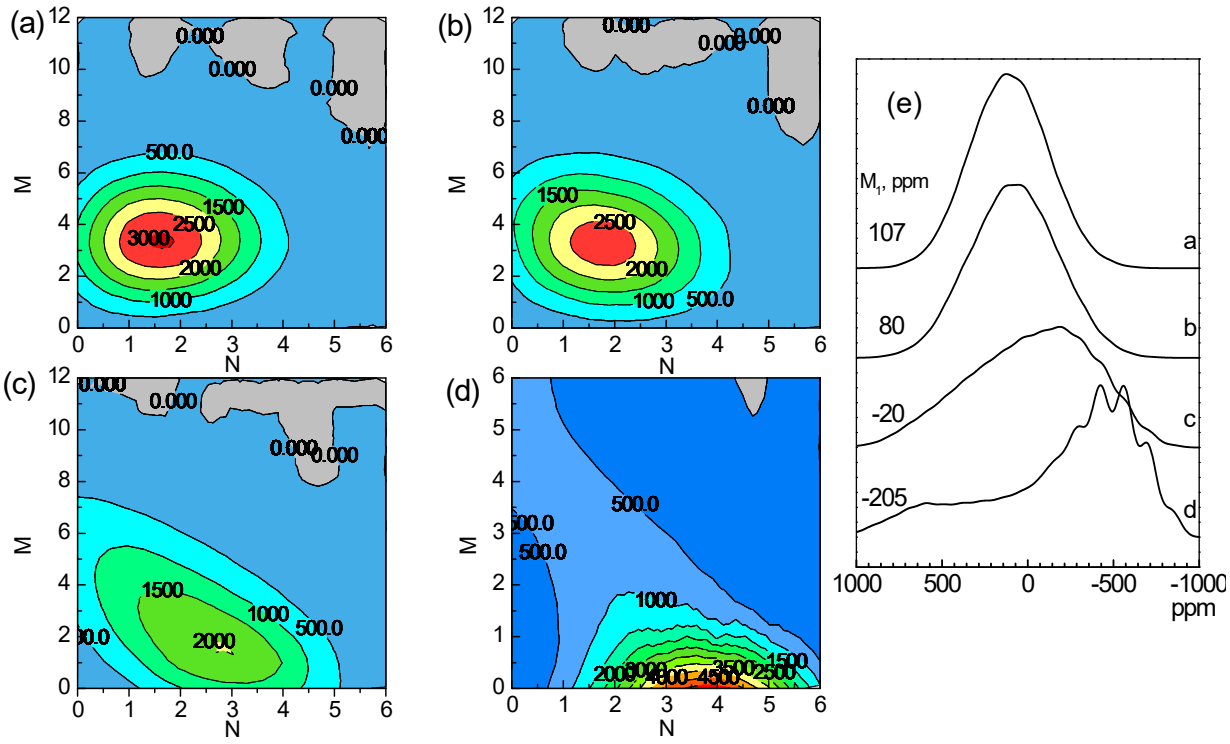

Fig. S7. The contour plots of the calculated distributions $\rho_{M,N}$ of Li-environments within the model for $Li_{1.2}Nb_{0.2}Mn_{0.6}O_2$ composition (a-d). The corresponding transformation (e) of the modeled ^{7}Li NMR spectral shape (spectra a-d correspond to distributions a-d).

A cubic grid of 50×50×50 atoms was stochastically filled with Li, Nb, Mn and O atoms so that the positions where i+j+k were even contained a metal while the odd positions were filled with oxygen. The numbers of Li environments with a certain number M (0-12) of Mn atoms at 90° bonds (Li-O-Mn) and the number N of 180° bonds were calculated. Each Mn neighboring a resonating Li by a 90° bond resulting in a δ_a Fermi contact shift while each 180° Mn neighbor shifts the signal to δ_b ppm (δ_a and δ_b have the opposite signs). The NMR spectrum was then modeled by the function $f(\omega) = \sum_{M,N} \delta(\omega - M\delta_a - N\delta_b)\rho_{M,N} g(\omega)$, where δ is the delta-function and g(ω) is the Gaussian widening function which was chosen to have a constant half-width β of order of δ_a and δ_b independent on the number of paramagnetic neighbors of lithium. The spectra shown in **Fig. S5 (e)** were calculated using δ_a = 100, δ_b = -140 and β = 120 ppm.

(a) $Li_{1.2}Ti_{0.4}Mn_{0.4}O_2$ (b) $Li_{1.3}Nb_{0.3}Mn_{0.4}O_2$

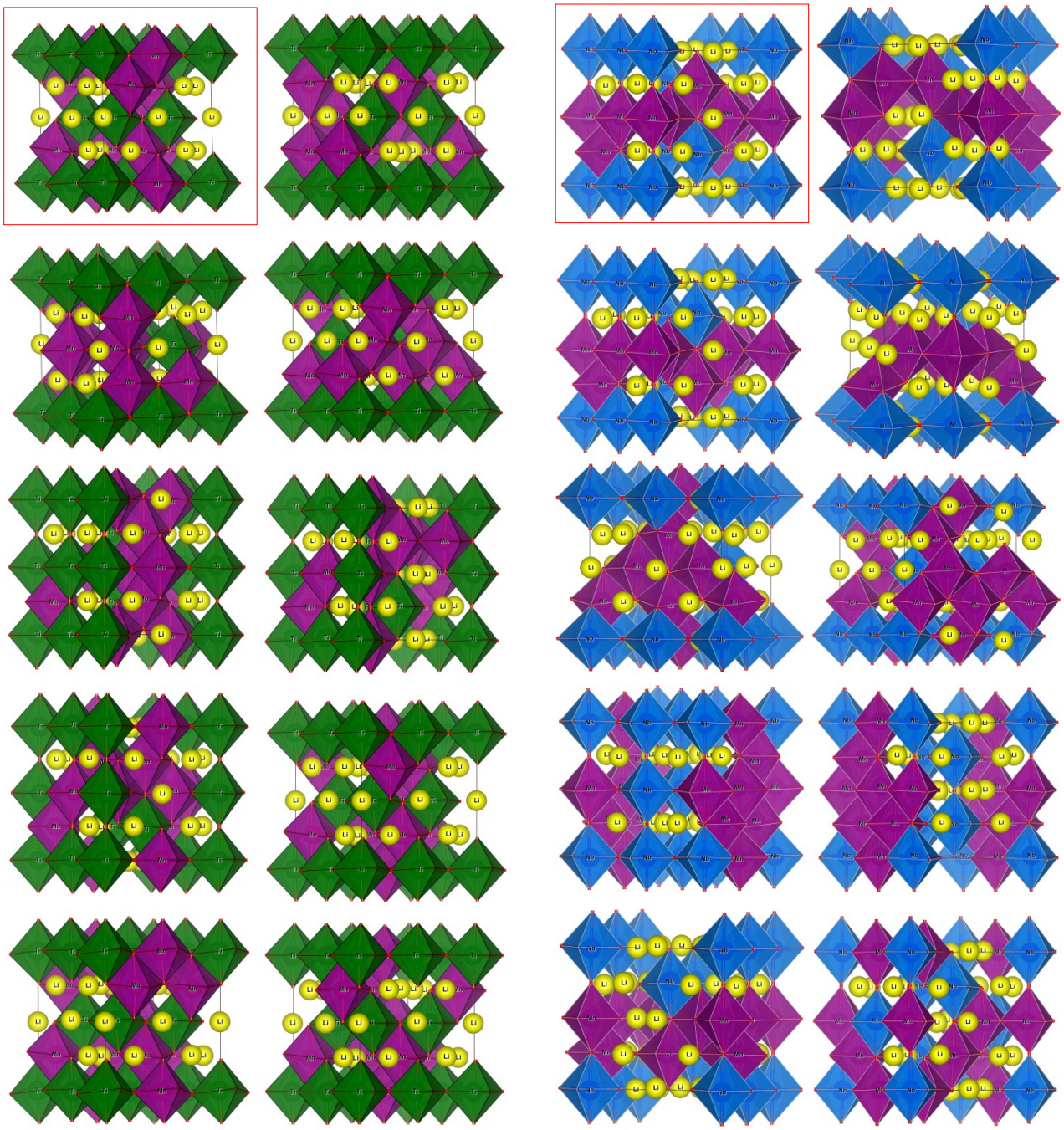

Fig. S8. All the ten lowest energy configurations of $Li_{1.2}Ti_{0.4}Mn_{0.4}O_2$ (a) and $Li_{1.3}Nb_{0.3}Mn_{0.4}O_2$ (b) compositions generated using a supercell program after optimization using DFT. Those ones used for the study of the Li migration paths by NEB method are in the red boxes.

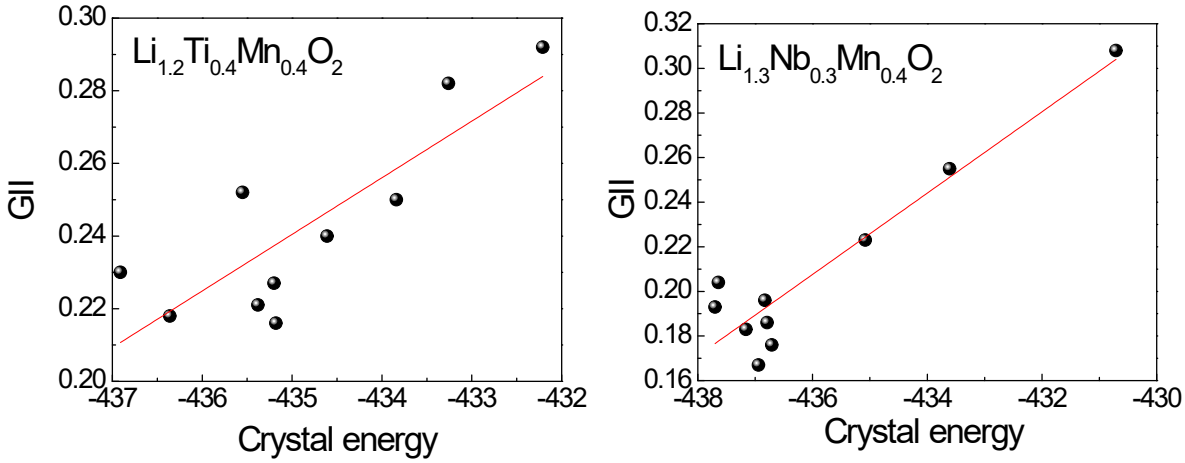

Fig. S9. Correlation between GII factor and crystal energy defined by DFT optimization for each configuration.

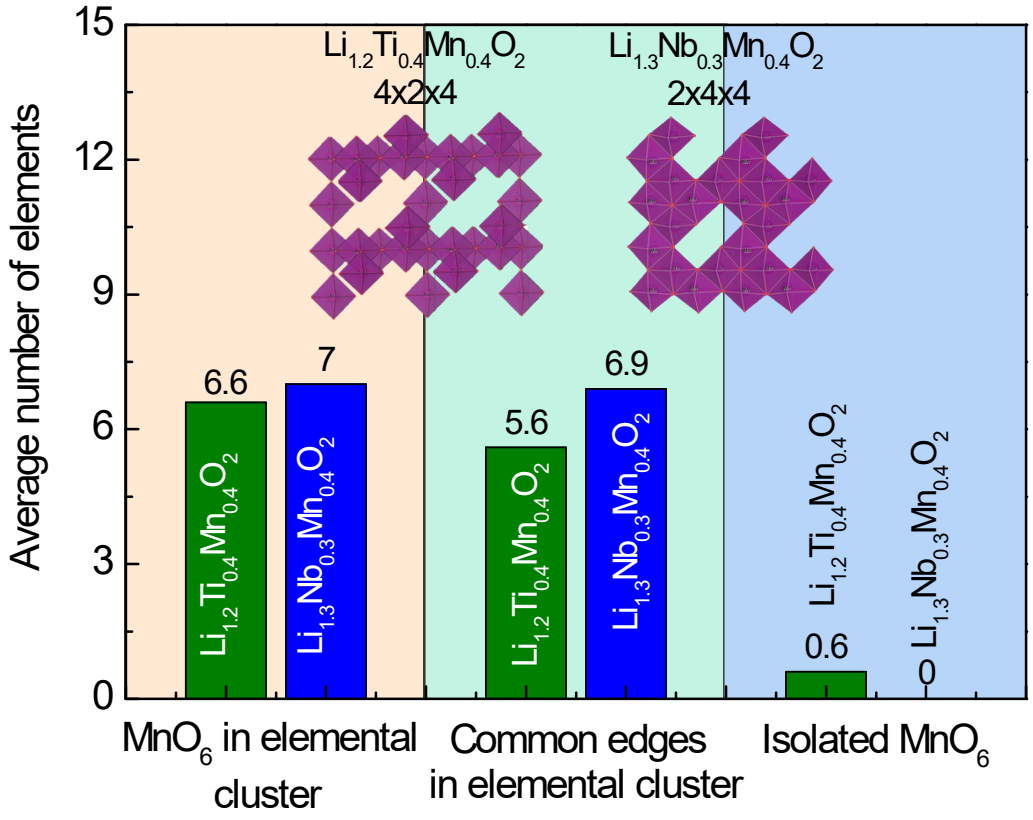

Fig. S10. Averaged over 10 configurations number of MnO_6 octahedra and common edges between them in an elemental cluster, and the average number of isolated MnO_6 in 2x2x2 unit cell. Insert: examples of Mn-clustering in $Li_{1.2}Ti_{0.4}Mn_{0.4}O_2$ and $Li_{1.3}Nb_{0.3}Mn0_{.4}O_2$.

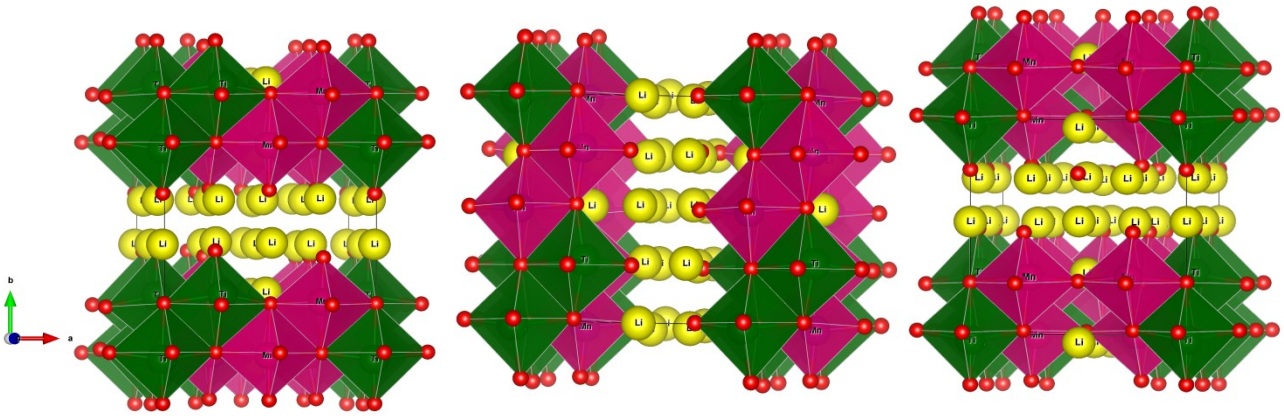

Fig. S11. The examples of three unstable configurations of $Li_{1.2}Ti_{0.4}Mn_{0.4}O_2$.

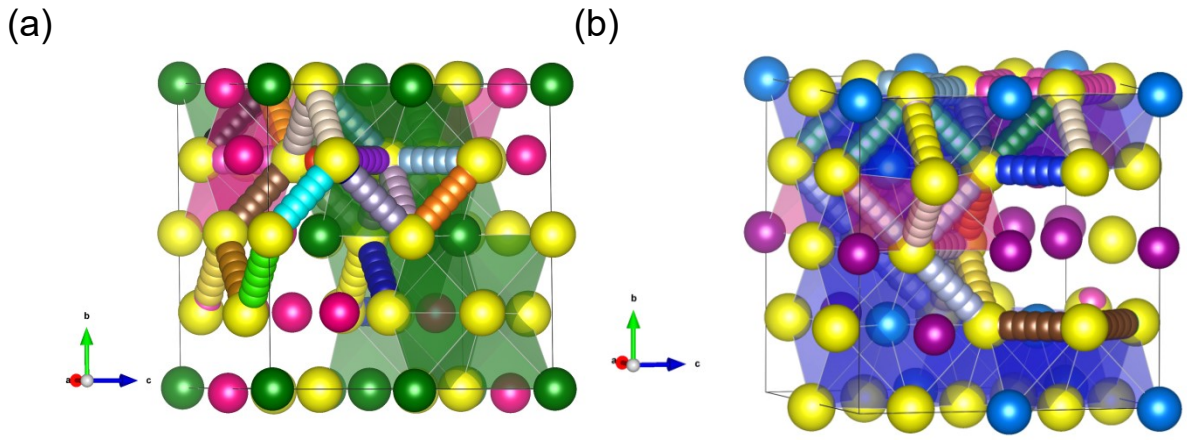

Fig. S12. Migration maps of $Li_{1.2}Ti_{0.4}Mn_{0.4}O_2$ (a) and $Li_{1.3}Nb_{0.3}Mn_{0.4}O_2$ (b) in 2*2*2 supercells.

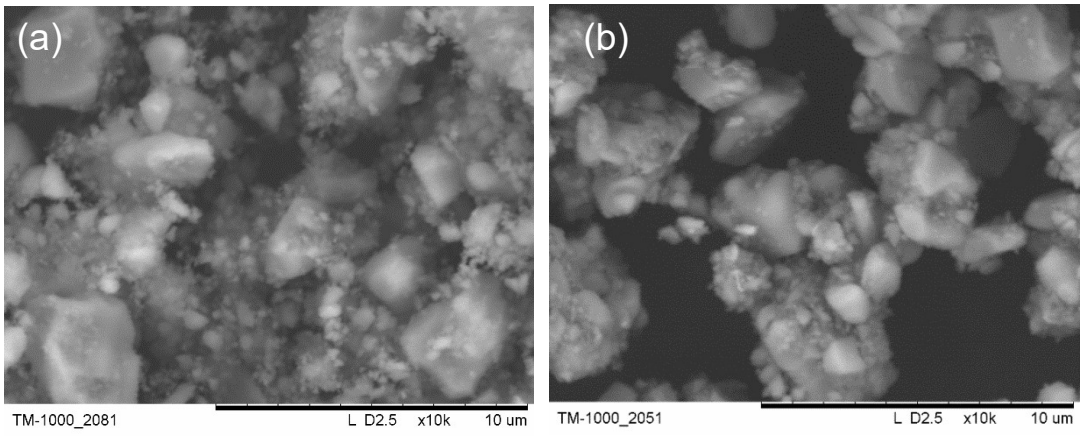

Fig. S13. SEM images of $Li_{1.2}Ti_{0.4}Mn_{0.4}O_2$ (a) and $Li_{1.3}Nb_{0.3}Mn_{0.4}O_2$ (b).

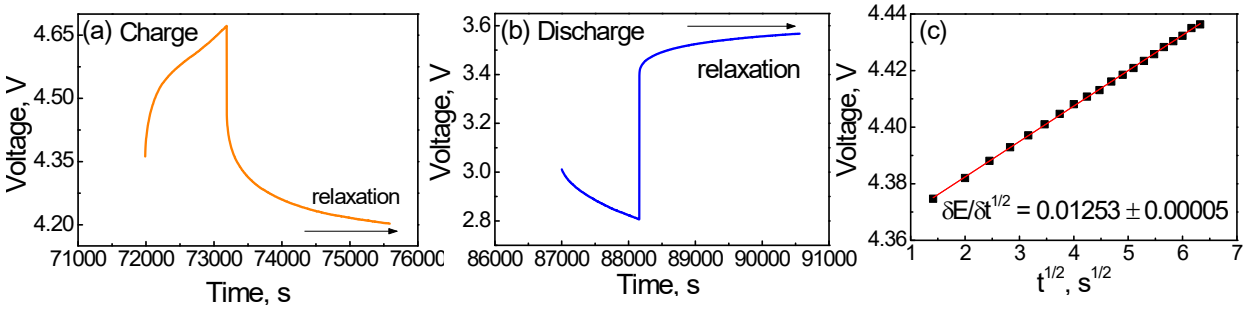

Fig. S14. Examples of voltage vs. time profiles for a single GITT titration at the state of charge (a) and discharge (b); voltage vs. $t^{1/2}$ plot (c).